Small Angle Neutron Scattering Studies of Phase Equilibria in Blends of Deuterated Poly(methyl methacrylate) with Solution Chlorinated Polyethylene

J. N. Clark,† M. L. Fernandez, P. E. Tomlins,‡ and J. S. Higgins*

Department of Chemical Engineering, Imperial College, London SW7 2BY, U.K.

Received May 25, 1993; Revised Manuscript Received August 4, 1993•

ABSTRACT: Blends of deuterated poly(methyl methacrylate) with solution chlorinated polyethylene have been studied by small angle neutron scattering. The effects of varying molecular weight and chlorination level have been ascertained on the polymer–polymer interaction parameters obtained as well as on the position of the spinodal curves. The blend was studied both in the one-phase and in the two-phase regions of the phase diagram. For the dPMMA-rich compositions the phase separation mechanism appeared to be spinodal decomposition. For compositions rich in SCPE the mechanism of phase separation was nucleation and growth. For certain compositions evidence has been found for incompatibility in the polymer–polymer system arising from the sample preparation.

Introduction

The technological importance of polymer blends has long been recognized by polymer scientists. By mixing two or more polymeric species it may be possible to produce new materials with desirable properties possessed by neither of the constituent polymers separately. Blending technology relies on miscibility although often total compatibility in a thermodynamic sense is not the aim. Nevertheless the thermodynamics of mixing are crucial in understanding the miscibility of polymers.

The configurational entropy of mixing for high molecular weight species is so small that in order to achieve miscibility a negative heat of mixing is often necessary; consequently, a large number of polymer pairs derive their miscibility from some specific interaction, giving a negative enthalpy of mixing. In order to study polymer miscibility the dependence of the Gibbs free energy of mixing (ΔG_m) on temperature, composition, and molecular weight has to be determined. Small angle neutron scattering is one of the most powerful methods[1] for obtaining ΔG_m, and from such measurements an effective polymer–polymer interaction parameter, χ_{eff} can be extracted directly.

Miscibility in blends of chlorinated polyethylene (CPE) or poly(vinyl chloride) (PVC) with poly(methyl methacrylate) (PMMA) has usually been attributed to a specific attractive interaction between the carbonyl group of the PMMA and the α-hydrogen of CPE/PVC. This interaction is generally thought to be due either to hydrogen bonding[2-4] or to a Lewis acid–base interaction.[5-7] However, a dipole–dipole interaction between the carbonyl group of the PMMA and the C–Cl bond of the CPE cannot be ruled out, since blends of PMMA and Saran (a chlorinated copolymer with very few α-hydrogens) have also been found to be miscible.[8-10]

It is not possible to compare quantitatively the results of studies of these blends from different laboratories since no two research groups work on exactly the same samples. The chlorination level of the CPE, the tacticity of the PMMA, the molecular weights of both components, the experimental technique, and the sample preparation methods are all parameters which vary, and all affect the observed miscibility of the blend.

PVC is about 57% by weight chlorine. Different chlorination levels can be obtained by chlorination of PVC or polyethylene (PE). Chlorinated PVC (CPVC) retains the regularity of the $[-CH_2-CClH-]_n$ repeat unit of the PVC while chlorination of PE gives rise to a more random structure which is consequently less prone to crystallization.[11] Two methods of chlorination are commonly used: suspension and solution. Suspension-prepared CPE is prone to a blocky, uneven chlorination due to surface-to-core variation, and therefore solution chlorination is often the preferred technique for making small batches of material. Chai *et al.*[12] studied the microstructure of solution CPE by ^{13}C NMR and differential thermal analysis (DTA). At chlorination levels greater than 50%, there were no detectable sequences of more than four adjacent methylene groups. In addition, CCl_2 groups first appear at a chlorination level of 50%. There was no evidence, from DTA measurements, of crystallinity in samples over 37% chlorine.

Vorenkamp and Challa,[6] Walsh *et al.*,[13] and Lemieux *et al.*[10] observed the effect of chlorination level on blend miscibility. Vorenkamp and Challa[6] carried out light scattering, infrared spectroscopy and DSC measurements on blends of PVC/PMMA and CPVC/PMMA, and they also measured heats of mixing of low molecular mass analogues. They found that 63% CPVC was more miscible with PMMA than either nonchlorinated PVC or 65% CPVC, since the cloud point curve for the former was shifted to higher temperatures than for the nonchlorinated PVC or for the 65% CPVC. They suggest that chlorinating from 57% to 63% increases the number of CClH groups which are involved in specific interactions, thus improving miscibility, while at higher chlorination levels (above 63%), the number of CCl_2 groups becomes significant and these bulky groups weaken the intermolecular interaction through steric hindrance. Walsh *et al.*,[13] studying blends of PMMA with SCPE containing around 50% chlorine, also reported improved miscibility (*i.e.* higher phase separation temperatures) for blends with higher chlorine content. The techniques they used to determine miscibility were light scattering, dynamic mechanical measurements, and differential thermal analysis. They also measured the heats of mixing of oligomeric PMMAs and chlorinated octadecanes. The results of Lemieux *et al.*[10] are less easily interpreted because, in their measurements,

† Present address: Molecular Simulations, St. John's Innovation Centre, Cowley Rd, Cambridge CB4 4WS, U.K.

‡ Present address: National Physical Laboratory, Division of Materials Application, Teddington, Middlesex TW11 OLW, U.K.

• Abstract published in *Advance ACS Abstracts*, October 1, 1993.

0024-9297/93/2226-5897$04.00/0

the molecular weight of the 68% CPVC was more than double that of the unchlorinated PVC. Nevertheless in three out of five blends, the demixing temperature of the CPVC/PMMA, as seen by differential scanning calorimetry, was higher than for the PVC/PMMA blend for a given composition.

In this paper we describe the one-phase and two-phase behavior of blends of deuterated poly(methyl methacrylate) (dPMMA)/solution chlorinated polyethylene (SCPE) with varying molecular weights and varying chlorine levels, as seen by small angle neutron scattering (SANS). Thermodynamic parameters such as the second derivative of the Gibbs free energy of mixing and the interaction parameter have been obtained as a function of chlorine content of the SCPE and molecular weight of both dPMMA and SCPE. The results highlight the crucial role that specific interactions play in this blend.

Small Angle Neutron Scattering from Polymers

One-Phase Blends. The absolute coherent elastic scattering cross section, $\Delta\Sigma(q)/d\Omega$, for a one-phase mixture of two components 1 and 2 (which could be polymer–solvent or polymer–polymer) may be expressed by

$$\frac{d\Sigma(q)}{d\Omega} = V_1^{-1}(b_1 - \beta b_2)^2 S(q) \tag{1}$$

where V_i is the volume of a segment (one repeat unit) of component i, b_i is the coherent scattering length of a segment of component i, β is the ratio, V_1/V_2, q is the magnitude of the scattering vector, $\mathbf{q}$, and $S(q)$ is the molecular structure factor.[14]

According to Higgins and co-workers,[15-17] the small angle neutron scattering of a homogeneous, one-phase polymer blend of two components, in which a fraction of one polymer is deuterium labeled, is expressed by the following equation:

$$\frac{d\Sigma(q)}{d\Omega} = \frac{(cd + (1-c)h - \beta b)^2/V_1}{[\phi_1 N_1 P_1(q)]^{-1} + \beta[\phi_2 N_2 P_2(q)]^{-1} - 2\chi_{eff}} + \frac{c(1-c)(d-h)^2\phi_1 N_1 P_1(q)}{V_1} \tag{2}$$

where $d\Sigma(q)/d\Omega$ is the normalized coherent scattering as a function of q. h, d, and b are scattering lengths per repeat unit of the hydrogenous polymer 1, the deuterium labeled polymer 1, and the polymer 2, respectively, c is the volume fraction of polymer 1 which is deuterium labeled, ϕ_1 and ϕ_2 are the volume fractions of polymers 1 and 2 [$\phi_1 + \phi_2 = 1$], N_1 and N_2 are the degrees of polymerization, χ_{eff} is an effective interaction parameter per segment mole of polymer 1, and

$$P_i(q) = \frac{2}{(u+1)v^2}[(1+uv)^{-1/u} - 1 + v]$$

is the Debye scattering function where

$$u = \frac{M_{w_i}}{M_{n_i}} - 1$$

and

$$v = \frac{R_{g_i}^2 q^2}{2u+1}$$

M_w and M_n are the weight average and number average molecular weights and R_g is the z average radius of gyration. For $qR_g < 1$ (*i.e.*, the so called Guinier[18] or Zimm[19] range), the functions $P_i(q) \to 1 - (q^2R_{g_i}^2/3)$ so that in this range the intensity should vary linearly with q^2.

Equation 2 is the result of the application to a somewhat more complicated problem of the random phase approximation (RPA) proposed by deGennes[20] and Binder:[21]

$$[S(q)]^{-1} = [\phi_1 S_1(q)]^{-1} + [\phi_2 S_2(q)]^{-1} - 2\chi_{eff} \tag{3}$$

where $S_i(q)$ are the structure factors of species 1 and 2 and $S(q)$ is the total structure factor. Equation 3 is recovered by putting $d = h$ in eq 2.

For a two-component blend where all of one of the species is deuterated ($c = 1$), the second term of eq 2 is absent and small angle scattering arises only from the concentration fluctuations of 1 and 2 in the blend. In the limit of $q \to 0$, $P(q) \to 1$ and the scattered intensity is inversely proportional to the second derivative of the Gibbs free energy of mixing per lattice site divided by $\kappa_B T$, G''

$$\frac{d\Sigma}{d\Omega}(q\to 0) = \frac{(cd + (1-c)h - \beta b)^2/V_1}{[\phi_1 N_1]^{-1} + \beta[\phi_2 N_2]^{-1} - 2\chi_{eff}} = \frac{(cd + (1-c)h - \beta b)^2/V_1}{G''} \tag{4}$$

where

$$G'' = \frac{\partial^2(\Delta G_m/\kappa_B T)}{\partial\phi^2} = \frac{1}{N_1\phi_1} + \frac{\beta}{N_2\phi_2} - 2\chi_{eff} \tag{5}$$

χ_{eff} can be obtained from eq 2 or 3 in two ways. If the degrees of polymerization and radii of gyration of components 1 and 2 in the blend are known, one could fit the entire $d\Sigma(q)/d\Omega$ *vs* q curves by adjusting the parameter χ_{eff}. Alternatively, since the functions $P_i(q) \to 1$ as $q \to 0$, a plot of $[d\Sigma(q)/d\Omega]^{-1}$ *vs* q^2 should yield a straight line whose intercept at $q = 0$ would give directly the value of G'' and therefore χ_{eff} (see eqs 4 and 5). In this case only the degrees of polymerization and volume fractions of the components of the blend need to be known *a priori*. The scattering curves obtained in the present work could successfully be extrapolated to zero q (ignoring some extra scattering at very small q values), and therefore the second analysis method was used. In both cases, the parameter χ_{eff} obtained is an "effective" interaction parameter which is different to that in Flory's original theory in that it is often composition dependent. The relation between χ_{eff} and the Flory–Huggins interaction parameter χ_{12} is given by

$$\chi_{eff} = \chi_{12} - (1-2\phi_1)\left(\frac{\partial\chi_{12}}{\partial\phi_1}\right) - \frac{1}{2}\phi_1(1-\phi_1)\frac{\partial^2\chi_{12}}{\partial\phi_1^2} \tag{6}$$

For some three-component blends, it is possible to choose a "contrast matched" composition such that

$$cd + (1-c)h - \beta b = 0$$

This allows the measurement of the molecular weight and the R_g of polymer 1 in the blend:

$$\frac{d\Sigma}{d\Omega}(q\to 0) = \frac{c(1-c)(d-h)^2\phi_1 N_1}{V_1} \tag{7}$$

and

$$\frac{d\Sigma(q)}{d\Omega} = \frac{c(1-c)(d-h)^2\phi_1 N_1 P_1(q)}{V_1} \tag{8}$$

This procedure was used in order to measure the radius of gyration of dPMMA in SCPE, and the results will be shown later.

Two-Phase, Two-Component Blends. Phase separation of blends can occur by two distinct mechanisms: nucleation and growth (NG) or spinodal decomposition (SD). The former occurs when phase separation takes place in the metastable region of the phase diagram and in this case a supercritical nucleus is needed in order to trigger phase separation. The spinodal decomposition mechanism takes place in the unstable region of the phase diagram and in this case any concentration fluctuation gives rise to phase separation. The fundamental characteristic of the early stages of SD is the distinctive morphology resulting from the phase separation which is a co-continuous and very regular structure. Thermodynamically, one particular concentration fluctuation with wavelength Λ_m is favored and grows much more rapidly than the rest. This is reflected in a scattering experiment by the appearance in the scattering curves of a peak whose maximum intensity is at $q = q_m = 2\pi/\Lambda_m$. SD in polymer mixtures has been successfully described theoretically by Cahn and Hilliard[22] and subsequently by deGennes[23] and Pincus.[24] The following equation for the dependence of q_m on thermodynamic parameters is obtained:

$$q_m^2 = -G''/4K \tag{9}$$

where K is defined as

$$K = \frac{1}{6}\left(\frac{R_{g_1}^2}{N_1\phi_1} + \frac{R_{g_2}^2}{N_2\phi_2}\right) \tag{10}$$

Therefore if the system phase separates by SD and the characteristic spinodal peak appears in the q range sampled by SANS, values for G'' can be obtained from scattering measurements in the two-phase region.

Two-phase systems which do not phase separate by SD can also be studied by SANS provided that the size of the phases falls in the necessary q range. The treatment of such data varies depending on the nature of the system under investigation, and there are a number of theoretical calculations which describe the expression for the scattering factor for a wide range of structures. Two of the most widely used expressions are due to Porod and Debye. The Porod expression is valid for homogeneous particles which have sharp boundaries with the matrix in which they are dispersed and have surface area A_p and volume V_p. The scattered intensity in this approximation is proportional to the surface-to-volume ratio of the particles, A_p/V_p.[14,25]

$$\frac{d\Sigma(q)}{d\Omega}q^4 = \text{constant} = 2\pi B'\frac{l}{\rho}\left(\frac{A_p}{V_p}\right) \tag{11}$$

where l is the concentration of particles of component 1 in a matrix of component 2, ρ is the density of the particle, and B' is the scattering contrast per unit volume:

$$B' = \left(\frac{b_1 - \beta b_2}{V_1}\right)^2 \tag{12}$$

The $[d\Sigma(q)/d\Omega]\,q^4$ term is taken as the ordinate intercept of a "Porod" plot, $[d\Sigma(q)/d\Omega]\,q^4$ against q. If the particles are spherical, then the A_p/N_p ratio is equal to $3/r$, where r is the particle radius.

Debye and co-workers[26,27] developed an expression similar to the Porod approximation but went on to modify it for the case of perfectly random form and distribution of phases:

$$\frac{d\Sigma(q)}{d\Omega} = \frac{k\bar{\eta}^2 a^3}{(1 + a^2q^2)^2} \tag{13}$$

where k is a constant, $\bar{\eta}^2$ is the mean square fluctuation in scattering power, and a is the Debye–Bueche correlation length. In the case where one phase is a dilute component in the second phase, a may be taken as a measure of the size of the dilute component. In the case of a more concentrated phase dispersion where it is more difficult to define the particle size, a better estimate of the phase sizes is obtained by converting a into the transverse chord lengths of Porod and Kratky[14,28] (Figure 1):

$$\bar{l}_1 = \frac{a}{\phi_2} \qquad \bar{l}_2 = \frac{a}{\phi_1} \tag{14}$$

where $\bar{l}_1$ and $\bar{l}_2$ are the average lengths of random chords passing through the two phases.

If a scattering curve follows the Porod law, a plot of $[d\Sigma(q)/d\Omega]^{-0.5}$ against q^2 will yield a straight line where the value of the correlation length, a, can be found from the slope/intercept ratio of the line.

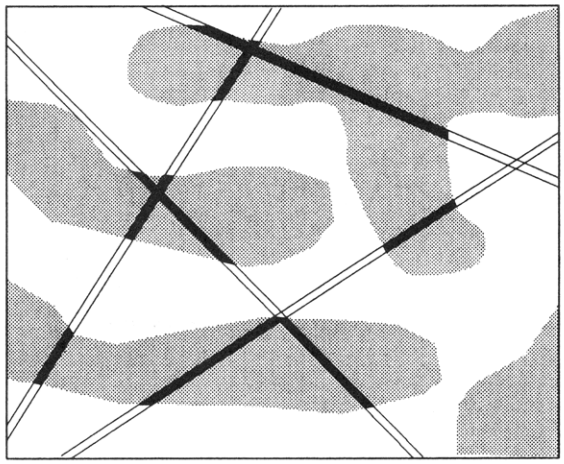

Figure 1. Schematic illustration showing random chords passing through two phases. The intersection lengths for each phase (black and white segments), averaged over many chords, are called the traversal lengths.[27,53]

Table I. Characteristics of SCPE Polymers

sample code	monomer mass (g mol^{-1})	scattering length (fm)	density (g cm^{-3})	M_w	M_n	Cl per monomer
SCPE63/1	72	15.4	1.47	413 000	126 000	1.28
SCPE66/3	75	17.7	1.52	104 000	62 300	1.45
SCPE64h	74	16.2	1.50	322 000	104 000	1.34
SCPE641	74	16.2	1.50	67 100	48 100	1.34
SCPE60	67	13.5	1.49	189 000	61 400	1.13

Experimental Section

Materials. Some of the basic characteristics of the polymers used in this work are listed in Tables I and II. The solution chlorinated polyethylenes were made by photochlorination[29,30] of a solution of linear polyethylene in chlorobenzene, details of which are published elsewhere,[13,31] and the samples were subsequently fractionated.[13,31] Using elemental analysis, the chlorine level was assessed by difference, subtracting the carbon and hydrogen content from the whole. The molecular weights of the SCPE's obtained are listed in Table I in polystyrene equivalents and were measured by GPC. Densities were found by density titration or by interpolation from a plot of density as a function of chlorination level.[31]

A very high molecular weight deuterated PMMA was supplied by Dr. H. Snyder of Dupont, U.S.A. Samples of lower molecular

Table II. Characteristics of PMMA Polymers

sample code	monomer mass (g mol^{-1})	scattering length (fm)	density (g cm^{-3})	M_w	M_n
hPMMA120	100	14.9	1.19	120 000	77 000
hPMMA64	100	14.9	1.19	63 600	33 000
dPMMA185	108	98.2	1.28	185 000	88 200
dPMMA810	108	98.2	1.28	810 000	313 000
dPMMA112	108	98.2	1.28	112 000	64 100
dPMMA33	108	98.2	1.22	33 000	15 000
dPMMA158	108	98.2	1.22	158 000	150 000

Table III. Blends of SCPE/PMMA, Compositions Given in Weight Percent

designation no.	SCPE66	dPMMA810
1	15	85
2	25	75
3	50	50

designation no.	SCPE63	dPMMA112
4	15	85
5	26	74
6	40	60
7	50	50

designation no.	SCPE64h	dPMMA185	hPMMA120
8	15	85	0
9	25	75	0
10	50	50	0
11	75	25	0
12	15	13	72

designation no.	SCPE641	dPMMA185
13	50	50

designation no.	SCPE60	dPMMA33
14	50	50

designation no.	SCPE60	dPMMA158
15	30	70

Table IV. Values Obtained for G'' and χ_{eff}

designation no.	ϕ_{SCPE}/ϕ_{dPMMA}	annealing temp (°C)	G''	χ_{eff}	$T_{spinodal}$ (°C)
		dPMMA810/SCPE66			
1	0.15/0.85	97	0.00016	0.004	
"	"	spinodal	0.0	0.0049	
2	0.25/0.75	97	0.0091	−0.0021	
"	"	103	0.0046	0.00016	
"	"	108	0.0015	0.0017	
"	"	spinodal	0.0	0.0029	100 ± 1
3	0.50/0.50	97	0.091	−0.044	
"	"	108	0.065	−0.031	
"	"	120	0.037	−0.017	
"	"	spinodal	0.0	0.0012	144 ± 12
		dPMMA185/SCPE64h			
8	0.15/0.85	as cast	0.23	−0.11	
"	"	spinodal	0.0	0.0027	89.5 ± 8
9	0.25/0.75	as cast	0.19	−0.093	
"	"	spinodal	0.0	0.0017	89 ± 9
10	0.5/0.5	97	0.10	−0.049	
"	"	108	0.07	−0.034	
"	"	120	0.04	−0.019	
"	"	spinodal	0.0	0.0012	152 ± 24
11	0.75/0.25	97	0.22	−0.11	
"	"	108	0.15	−0.074	
"	"	120	0.11	−0.054	
"	"	150	0.039	−0.018	
"	"	spinodal	0.0	0.0015	170 ± 9
		dPMMA185/SCPE641			
13	0.50/0.50	as cast	0.42	−0.21	
"	"	100	0.16	−0.077	
"	"	spinodal	0.0	0.0026	
		dPMMA33/SCPE60			
14	0.50/0.50	96.4	0.085	−0.042	
"	"	101	0.054	−0.025	
"	"	105.7	0.039	−0.018	
"	"	110.4	0.022	−0.008	
"	"	114.1	−0.003	–	
"	"	spinodal	0.0	0.335	113.6
		dPMMA160/SCPE60			
15	0.70/0.30	91.7	0.008	−0.003	
"	"	105.7	−0.0036	–	
"	"	spinodal	0.0	0.0012	103.1

weights were subsequently prepared by exposing pieces of the high molecular weight dPMMA to controlled doses of γ radiation.[32] The original PMMA sample was prepared by free radical polymerization and therefore had predominantly atactic stereochemistry.[29] Sample dPMMA33 was purchased from Polymer Laboratories and was prepared by anionic polymerization. Its tacticity could therefore be slightly different from that for the rest of the samples.

SCPE/dPMMA blend samples were made by solution casting 2–5% weight by volume solutions of polymer in methyl ethyl ketone (MEK) or chlorobenzene. The tacky films were then held in a 40–60 °C vacuum oven until dry, and the resulting cast films were typically 0.1–0.25 mm thick.

A list of the SCPE/dPMMA samples prepared is presented in Table III. All compositions are given in weight percent. Sample 12 is contrast matched such that the coefficient of the leading term in eq 2 is zero. Therefore the scattered intensity arises only from the single chains and there is no contribution to the scattering from the concentration fluctuations in the system. This sample was prepared in order to measure the molecular weight and radius of gyration of dPMMA in a dPMMA/SCPE blend and to compare this value with the literature radius of gyration of dPMMA in hPMMA.

Samples for SANS were prepared by stacking disks, cut from the cast film, up to the required thickness, which was of the order of 1 mm. For SANS experiments, samples 1–13 were measured at ambient temperature. Samples were prepared before the experiment by annealing and quenching. The stacked film samples were sandwiched between clean aluminum sheets and lightly clamped before annealing. Annealing temperatures are given in Table IV and the annealing times were typically 30 min for the thinner samples and 2 h for the thicker specimens. Samples were quenched, in iced water, immediately upon removal from the oven. Samples 14 and 15 were measured "at temperature", the stacked disks cut from the cast films being enclosed in brass cells with quartz windows which were placed directly in the neutron beam. The temperature stability in the cell was better than 0.1 deg. The heating setup was calibrated, and the temperatures reported for the SANS measurements correspond to the real temperatures inside the cell. Prior to the SANS measurements the samples were allowed to equilibrate at the required temperatures for periods of time ranging from 30 min to 5 h depending on their position in the heating rack. Transmission measurements carried out on the samples at the beginning and at the end of the annealing process were similar, and therefore the annealing time was not thought to influence the results once the samples had been heated for a sufficient length of time to reach equilibrium.

Glass transition temperatures for the homopolymers and the as-made blends were measured by differential scanning calorimetry (DSC) and are plotted in Figure 6b.

Small Angle Neutron Scattering Measurements. SANS measurements were made on diffractometers D17 and D11 at the Institute Laue-Langevin in Grenoble and on the LOQ instrument at the ISIS pulsed source Rutherford Appleton Laboratory in Oxfordshire.[33] For the measurements carried out in D11 and D17, water, an empty water cell, an empty sample holder, and the hydrogenous component polymers were all measured in addition to the blend samples of interest. Using the scattering from water, the data were corrected for detector efficiency and the scattering was normalized to absolute units. Because the LOQ spectrometer uses pulsed multiwavelength neutrons, absolute intensities are calculated in a slightly different way than for reactor sources. Details on the experimental setup and on data analysis can be found in ref 34. In all cases, the parasitic scattering from the sample holder was subtracted from

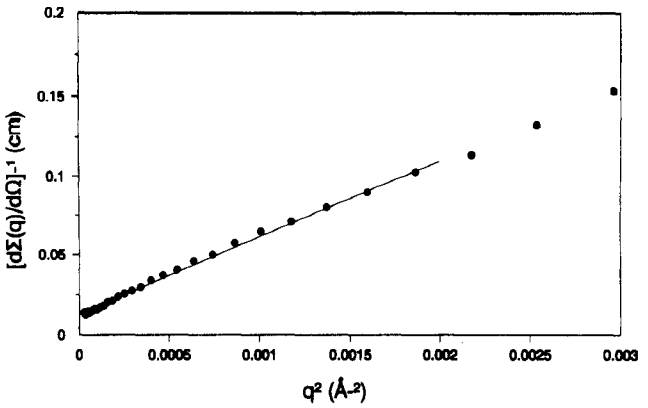

Figure 2. SANS for contrast matched sample SCPE64/dPMMA185/hPMMA120 (blend 12), $[d\Sigma(q)/d\Omega]^{-1}$ against q^2 plot: (●) data points and (—) least squares fit.

the sample scattering and the incoherent scattering backgrounds were estimated from the scattering of the hydrogenous polymers. The data normalization was checked using standard blends with known molecular weights. The standard used for samples 1–13 was a mixture of hydrogenous and perdeuterated PMMA. This dPMMA/hPMMA sample was not available at the time of running the measurements on samples 14 and 15 and a perdeuterated polystyrene/hydrogenous polystyrene standard was used instead. Data analysis was then carried out using the standard programs.[34,35]

Before corrected, normalized, scattering data can be interpreted using eqs 2–14 above, it is necessary to remove the q independent, incoherent scattering from the total scattering. The primary source of incoherent scattering in these experiments is hydrogen. In a blend containing both hydrogenous and deuterium labeled polymers, removal of the incoherent background scattering may be accomplished by measuring the scattering due to the hydrogenous polymer alone and subtracting an appropriate fraction of the scattering curve from that of the blend. The appropriate fraction is often taken as the volume fraction of hydrogen containing material in the sample[36] but is more correctly found by comparing the transmissions of the two materials[17]

$$\left(\frac{d\Sigma}{d\Omega}\right)_{coh} = \left(\frac{d\Sigma}{d\Omega}\right)_{tot} - \left[\frac{(1-T_s)d_hT_h}{(1-T_h)d_sT_s}\right]\left(\frac{d\Sigma}{d\Omega}\right)_h \quad (15)$$

where $(d\Sigma/d\Omega)_{coh}$ is the coherent scattering from a sample containing both hydrogenous and deuterium labeled polymer, $(d\Sigma/d\Omega)_{tot}$ is the normalized experimental scattering of the above sample, $(d\Sigma/d\Omega)_h$ is the normalized experimental scattering from the hydrogenous polymer, T is the transmission, d is sample thickness, s refers to the sample of interest and h refers to the nonlabeled sample.

Results and Discussion

(1) Contrast Matched Sample—Single Chain Dimensions. The scattering from the contrast matched sample (12) of SCPE64/dPMMA185/hPMMA120 was measured in the instrument LOQ in order to determine the R_g of dPMMA185 in a blend with SCPE and to compare this R_g with the literature value for dPMMA185 in a blend with hPMMA. In Figure 2, the values of $[d\Sigma(q)/d\Omega]^{-1}$ are plotted against q^2 for the hSCPE64/dPMMA185/hPMMA120 sample along with the least squares fit of the data points to eq 7. Data were collected over a large q range and the linearity of the $[d\Sigma(q)/d\Omega]^{-1}$ *vs* q^2 plots was so good that it was possible to fit straight lines up to fairly large values of q^2. The plots were linear over such a large q range because the polydispersity, u, of the PMMAs was very near 1 (see Table II), and in this case a Zimm plot corresponds exactly to a straight line.[37] Data fitting was carried out above the Zimm range (*i.e.* above $qR_g = 1$), and the apparent values obtained for the radius of gyration and the molecular weight were corrected according to Ullman's[38] procedure. The molecular weights of the dPMMA and hPMMA were slightly dissimilar, and the data were also corrected for this mismatch following the procedure of Boue *et al.*[39] and Crist *et al.*[40]

Two fitting ranges were used: from $q^2 = 3 \times 10^{-5}$ to 2×10^{-3} Å^{-2} (*i.e.* $0.61 \le qR_g \le 5$) and from 3.8×10^{-4} to 0.012 Å^{-2} (*i.e.* $2.2 \le qR_g \le 12.2$). When the first fitting range was used, (which is the only one shown in Figure 2), the values obtained for R_g and the weight average molecular weight, M_w, were 109 Å (3% smaller than the bulk dPMMA value[41]) and 1.72×10^5 (93% of the GPC value polystyrene equivalent). The results obtained from the second fitting range were R_g = 110 Å (2% smaller than the bulk PMMA value) and $M_w = 1.79 \times 10^5$ (97% of the GPC value). We can therefore conclude that, within experimental error, the radius of gyration of the dPMMA is not affected by blending. It is worth pointing out that sometimes it is better to collect data over a large range of q and to fit the points outside the Zimm range in order to avoid complications that frequently arise at low q such as the presence of voids or microheterogeneities. This point will be emphasized later.

(2) Phase Behavior of SCPE/dPMMA. Determination of G'' and χ_{eff}. Figure 3 shows a plot of intensity against q for blend 14 as a function of annealing temperature. The bottom curve corresponds to the scattering from a sample of SCPE60 at room temperature (the sample was also run at 118 °C, and the scattering profile was identical to that at room temperature). The next four curves correspond to the blend SCPE60/dPMMA33 at different annealing temperatures inside the one-phase region. As predicted by eq 4, the scattered intensity increases with the annealing temperature since G'' reduces toward zero as the spinodal is approached. The two top curves correspond to the same blend inside the two-phase region, and the scattering shows typical spinodal peaks, the lower of the two curves corresponds to an annealing temperature of 114 °C and the upper one to 118 °C. Further details on the two-phase behavior of the blend will be introduced later.

As explained earlier, the inverse of the scattered intensity should vary linearly with q^2 in the small q range, $qR_g \le 1$. According to eq 4, G'' and χ_{eff} can be obtained from plots of $[d\Sigma(q)d\Omega]^{-1}$ *vs* q^2 extrapolated to $q = 0$. In Figure 4 plots of $[d\Sigma(q)/d\Omega]^{-1}$ against q^2 for blend 14 in the one-phase region are shown as an example together with the best fits. The results of G'' and χ_{eff} obtained for all the blends are collected in Table IV. The values reported for χ_{eff} at the spinodal were calculated from eq 5 for $G'' = 0$, which is the definition of the spinodal. Intense scattering was seen at low q for all the SCPE-rich blends (here and thereafter, by "SCPE-rich" we will mean 50% or 75% by weight in SCPE), as in Figure 4, and the reasons for this will be explained later. We attribute this to parasitic scattering from residual phase separation, and as explained later, we believe we can analyze the data at higher q values in terms of eq 4. When data fitting was carried out outside the Zimm range, the results were subsequently corrected as described in the previous section.

In the Flory–Huggins approximation G'' should be linearly proportional to the inverse of the annealing temperature, T^{-1}, and zero at the spinodal. Spinodal temperatures can therefore be estimated by fitting G'' against T^{-1} plots. Examples are shown in Figure 5 for blends 14, 10, and 3.

The spinodal temperatures T_s obtained are shown in Table IV and represented in Figure 6a. The dotted line is a guide to the eye drawn through the experimental

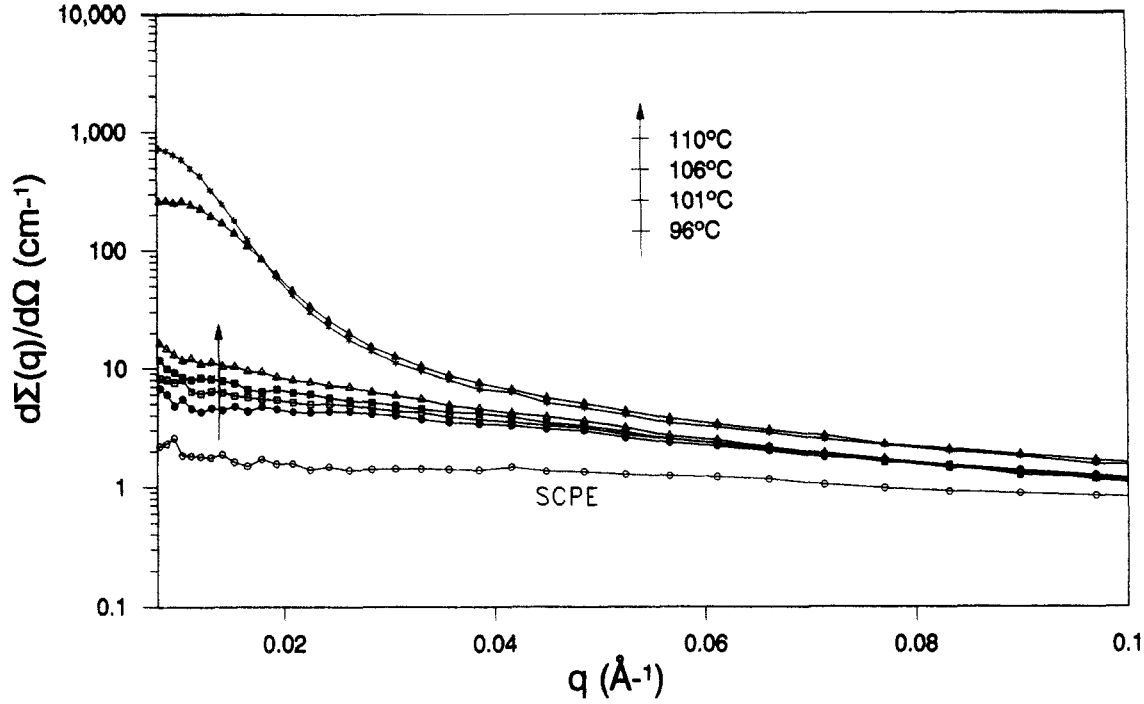

Figure 3. SANS patterns obtained for a SCPE60 sample (○) and for blend 14 at six different annealing temperatures. Four of the patterns correspond to the blend in the one-phase region: 96 °C (●); 101 °C (□); 106 °C (■); 110 °C (△). The two top curves correspond to the scattering from the same sample in the two-phase region: (▲) 114 °C; (*) 118 °C. For clarity, lines are shown connecting the experimental points.

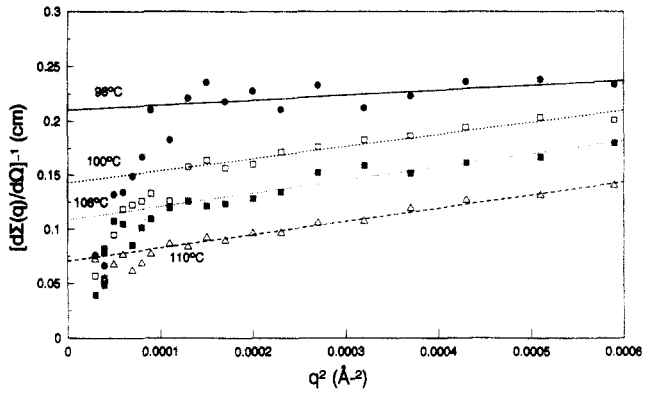

Figure 4. Plots of $[d\Sigma(q)/d\Omega]^{-1}$ against q^2 for blend 14 at four different temperatures in the one-phase region of the phase diagram. The lines correspond to the least squares fit to the data.

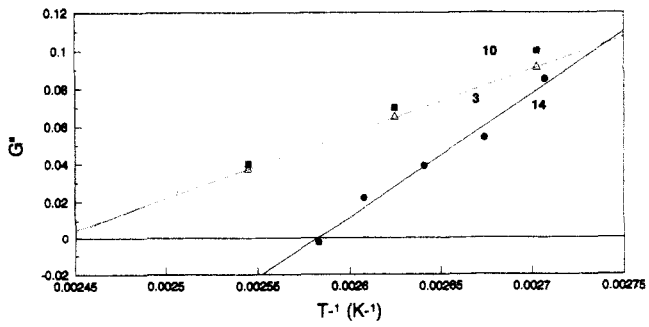

Figure 5. Plot of the second derivative of the Gibbs free energy of mixing as a function of the inverse of the temperature for blends 3, 10, and 14. The lines correspond to the least squares fit through the data points.

spinodal temperatures for the system SCPE66/dPMMA810 (blends 1–3) and the dashed line corresponds to the system SCPE64h/dPMMA185 (blends 8–11). The chlorination level of the SCPE for both systems is not too dissimilar, but the molecular weight of the dPMMA in the former system is much larger than in the latter. Within

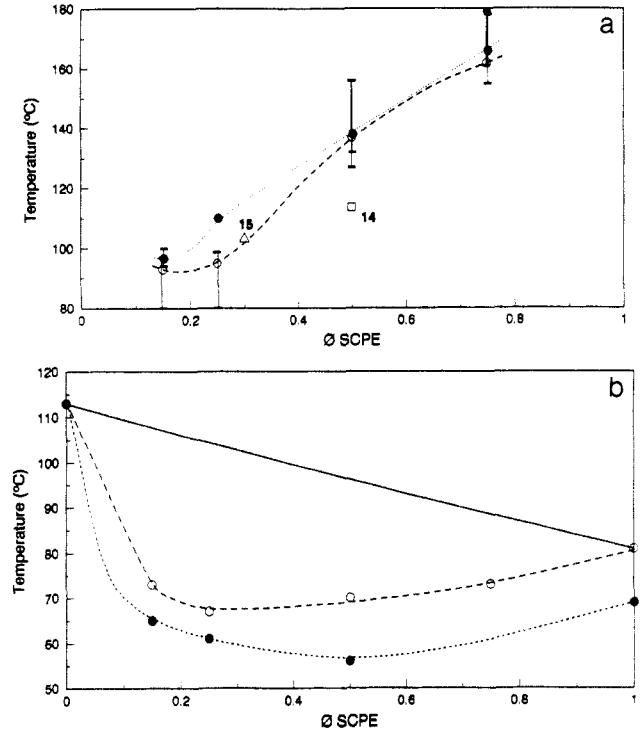

Figure 6. (a) Spinodal curves measured for the systems SCPE66/dPMMA810 (blends 1–3) (···●···) and SCPE64h/dPMMA185 (blends 8–11) (- - -○- - -). The point at $\phi = 0.75$ for blend SCPE66/dPMMA810 is from ref 2. The error bars have been slightly displaced for clarity. Also plotted are the spinodal temperatures measured for blends 14 (□) and 15 (△). (b) Glass transition temperatures measured for the systems SCPE66/dPMMA810 (···●···) and SCPE64h/dPMMA185 (- - -○- - -). For both figures the lines are guides to the eye through the experimental data. The solid line represents the curve for the Fox equation[41] for the system SCPE64h/dPMMA185. For clarity, the Fox curve for the second system is not shown.

experimental error, the spinodal curves for both systems are fairly similar, which indicates that the effect of the chlorine content in the SCPE is to improve the miscibility

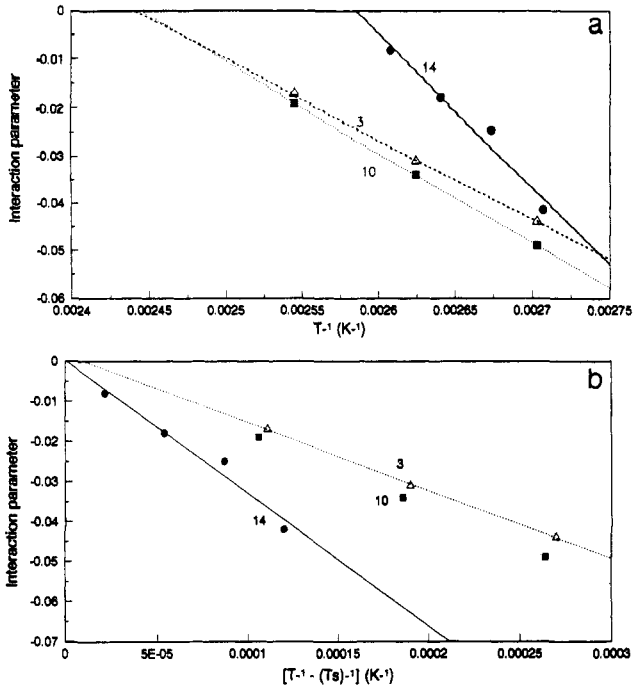

Figure 7. (a) Interaction parameter as a function of the inverse temperature for blends 3, 10, and 14. (b) Interaction parameter as a function of $(T^{-1} - T_s^{-1})$. The lines correspond to the best fit through the data points.

in the blend. In general, an increase in the molecular weight reduces the combinatorial entropy of mixing and therefore decreases the miscibility, but in the case of these two blends a 2% change in the chlorine content of the SCPE is enough to outweigh the effect of increasing the molecular weight of the dPMMA by 4 times. An even more dramatic example is shown by the data for blend 14, which corresponds to a 50% SCPE composition. In this case the spinodal temperature for blends 3 or 10 is approximately 34 deg higher than that for blend 14. Therefore, a 6% increase in the SCPE chlorine content more than balances a 25-fold increase in the molecular weight of the dPMMA. This demonstrates the large effect that the specific interactions have in this blend, which is also reflected in the large absolute values obtained for the interaction parameter χ_{eff}. Figure 6b shows the glass transition temperatures for various blends as measured by DSC, where the dotted and dashed lines have the same meaning as in Figure 6a. A comparison of both figures shows that the spinodal temperatures for both systems are higher than the glass transition temperatures and therefore the system shows a miscibility window. Also, the curves of glass transition against composition show a clear deviation from the Flory–Fox equation[42] (solid line) which indicates the presence of strong interactions in the blend.

Plots of χ_{eff} *vs* T^{-1} for the same data as in Figure 3 are shown in Figure 7a. In Figure 7b the same data are plotted in a slightly different way in order to decouple the position of the phase diagram from the temperature dependence of χ_{eff}. Values of the interaction parameter are plotted against $(T^{-1} - T_s^{-1})$ and therefore points with the same value of $(T^{-1} - T_s^{-1})$ correspond to points of equal quench depth outside the phase boundary.

It is clear that while the slopes of the lines for blends 10 and 3 are fairly similar, the slope for blend 14 is very different. The polymer composition for the three blends is the same (0.50/0.50), but the chlorine content of the SCPEs and the molecular weight of the dPMMAs are different. The different slopes for blends 10 and 3 and blend 14 could reflect a molecular weight dependence of the interaction parameter[43] below a certain value for the molecular weight of the dPMMA or a different strength of the specific interactions in the system due to the difference in the chlorination level of the SCPEs (again, the chlorine contents of the SCPEs in blends 3 and 10 are not too dissimilar, 66% and 64%, respectively, but that for blend 14 is markedly smaller, 60%). Finally, the difference between blends 3 and 10 and blend 14 could be due to a different tacticity of the dPMMAs, as explained in the Materials section. At present it is not possible to ascertain which of these factors is responsible for the effect observed, and a systematic set of measurements would be necessary to clarify this point. In the literature,[43] data for χ against T^{-1} are often fitted empirically as a function of composition, temperature, and molecular weight but no theoretical significance is attached to the parameters obtained.

From Table IV it is evident that χ_{eff} is strongly composition dependent although the amount of data available is not enough to make a complete study. As mentioned in the section on SANS from polymers and verified experimentally for some systems,[43] the interaction parameter obtained by SANS is an effective parameter which is in general composition dependent. Also from the table, it is apparent that the values for the blend containing the lower molecular weight SCPE (SCPE641) are more negative than those of the blend containing the higher molecular weight SCPE (SCPE64h) at the same temperatures and for the same composition and molecular weight of dPMMA. This could again be due to a molecular weight dependence of the interaction parameter or to a slight difference in the microstructure of the different SCPE fractions.

Another point worth mentioning is the fact that data for G'' *vs* T^{-1} for blend 14 (see Figure 5) contain not only points in the one-phase region of the phase diagram but also a point from the two-phase region. As explained in the theoretical section, this point was calculated from the maximum q_m in the curve of $d\Sigma(q)/d\Omega$ *vs* q, corresponding to a spinodal peak. Frequently, values of T, obtained from plots of G'' *vs* T^{-1}, have large errors because in cases when there is a lack of data near the spinodal temperature, long extrapolations are necessary. This is reflected for example in the large error bars in Figure 6a. By collecting data on both sides of the phase boundary, the extraction of the spinodal temperature is more accurate and errors are minimized. This procedure has already been successfully used by two of the authors on other systems.[44]

Excess Scattering at Low q. We have already mentioned excess scatter at low q as in Figure 4 and we now want to consider its origin. Our first experiments on the SCPE/PMMA blend were performed using the D11 diffractometer. This instrument, with its very low q access, was chosen because we were particularly interested in measuring the scattering of the blend in the q range where $qR_g \leq 1$. All the SCPE-rich samples were found to scatter excessively at low q, and the scattering could not be simply interpreted. Figure 8 shows a typical scattering profile obtained from one of the blends measured during this experiment. Subsequent measurements were carried out on D11, D17, and LOQ and again intense excess scattering was observed at low q values.

There are a few reports in the literature of curved plots of $[d\Sigma/d\Omega]^{-1}$ against q^2 in SANS from polymer blends. In most cases where $[d\Sigma/d\Omega]^{-1}$ against q^2 plots are reported to deviate from linearity at low q values, it is in the opposite sense to those described in the present work.[45,46] One

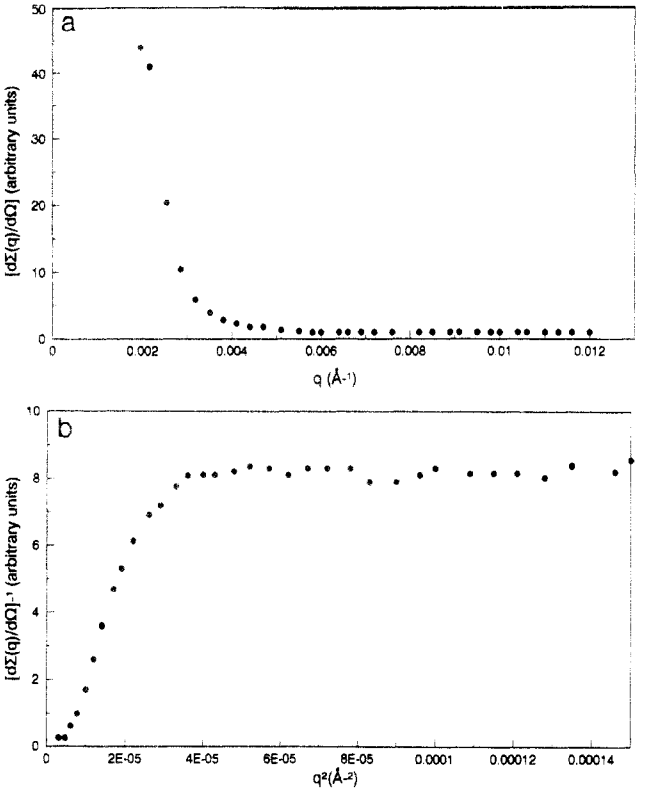

Figure 8. SANS pattern for SCPE63/dPMMA112 (blend 7) at 112 °C: (a) plot of $[d\Sigma(q)/d\Omega]$ against q; (b) plot of $[d\Sigma(q)d\Omega]^{-1}$ against q^2.

possible source of excess intensity at small angles is scattering from voids in the sample,[47] which would be expected to follow Porod's law. Indeed some workers[48,49] have used an additional q^4 term to describe the intensity:

$$\left(\frac{d\Sigma(q)}{d\Omega}\right)^{-1} = \left(\frac{d\Sigma(0)}{d\Omega}\right)^{-1} + b_1q^2 + b_2q^4 \qquad (16)$$

when fitting data which does not obey the simpler q^2 dependence, where $d\Sigma(0)/d\Omega$ is the scattered intensity extrapolated to $q = 0$. This did not fit satisfactorily to the SANS data for the SCPE/dPMMA blends and therefore voids or voids alone are not thought to be the cause of the excess intensity.

Maconnachie *et al.*,[17] in a study of a blend of poly(2,6-dimethyl-1,4-phenylene oxide) with either polystyrene or poly(4-methyl styrene), attributed the cause of curved $[d\Sigma(q)/d\Omega]^{-1}$ against q^2 plots to uneven quenching. Because of the large difference between the annealing temperature, T_a, and the T_g of the blend, the postanneal quench was not quick enough to arrest the finer structure of the blend at T_a. The result was that the scattered intensity at the lowest q values represented concentration fluctuations in a blend "frozen" at T_a, while at high q, the intensity was equivalent to that of a blend frozen at T_g. At intermediate q values, the scattered intensities are related to blends frozen at fictive temperatures between T_a and T_g. This resulted in plots of $[d\Sigma(q)d\Omega]^{-1}$ against q^2 which were smoothly curved over a large q range rather than showing distinct linear and curved regions, as in our case. It is not likely that uneven annealing is the cause of the excess scattering in the SCPE/dPMMA blends, as the difference between T_a and T_g in these blends is relatively small and because a normal variation of G'' with temperature was observed. However, in order to determine the influence of quenching on the scattering behavior in the system, samples 14 and 15 were tested "at temperature"; *i.e.* the samples were not quenched, but instead,

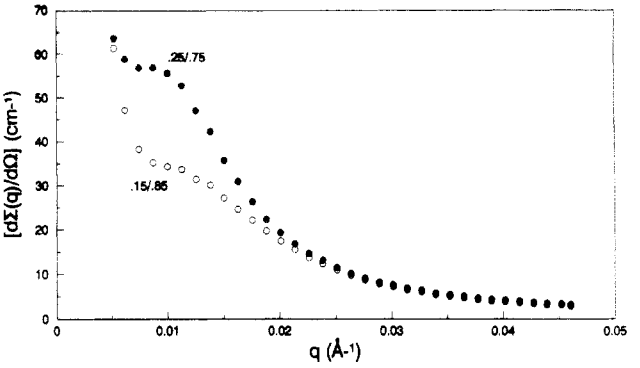

Figure 9. Scattering from blend samples of SCPE64h/dPMMA185; incipient spinodal decomposition: (●) blend 9; (○) blend 8.

annealing took place directly in the neutron beam and samples were equilibrated for longer times than those for the previous samples. As it is clear, for example, from Figure 4 for sample 14, excessively high intensity at low q values is still observed. As the temperature was increased, the linearity in plots of $[d\Sigma(q)/d\Omega]^{-1}$ against q^2 improved, which would be consistent for example with an "annealing out" of inhomogeneities present in the samples as cast.

Hahn[50] has also found scattering curves very similar to these for blends of poly(styrene acrylonitrile) with dPMMA. He also noted a composition dependence of the excess low q scatter; $[(d\Sigma(q)/d\Omega)]^{-1}$ against q^2 plots for blends with dPMMA compositions above 50% were found to be linear, but those samples with dPMMA compositions between 5% and 30% dPMMA showed excessive low q scatter which could be described with a Debye–Bueche model. The behavior of the 40% blend could go either way, depending on the sample preparation and annealing method. He was not able to explain the origin of this excess scatter.

It seems likely that the excess scatter in our system can be interpreted as phase separation. To demonstrate this, we need to discuss mechanisms and what we should expect from phase separated systems. The blends of 15% and 25% SCPE, 1, 2, 8, and 9, all appeared to phase separate by spinodal decomposition. All these blends were in the dPMMA-rich region, near the critical temperature, where the metastable region is very small. Distinct scattering peaks at q values below $\sim 1.2 \times 10^{-2}$ Å^{-1} were noted for samples heated above their spinodal temperatures; typical scattering curves for samples in the early stages of spinodal decomposition are shown in Figure 9. In Figure 10 we show a sample undergoing spinodal decomposition through several stages. In the early stages of phase separation the spinodal peak increases in intensity but remains at constant q; see Figure 10, II → III. In the later stages, the peak continues to grow in intensity but also shifts to smaller q values, (Figure 10, III → IV).

No spinodal peaks were seen for blends 50% and 75% SCPE, even when heated above T_g. These blends were in the SCPE-rich side of the phase diagram, far away from the critical composition and therefore in a region where there is a wide metastable gap. The scattering curves of phase separated blends of the 50% and 75% SCPE compositions were marked by very intense scatter at low angles and sometimes by a reduced scatter at higher angles, as in Figure 11a,b. The phase separated blend in Figure 11a (blend 11 at 150 °C) shows intense scattering across the q range. This suggests that the phase separated regions in the system contain some concentration fluctuations of small wavelength and large amplitude. On the other hand,

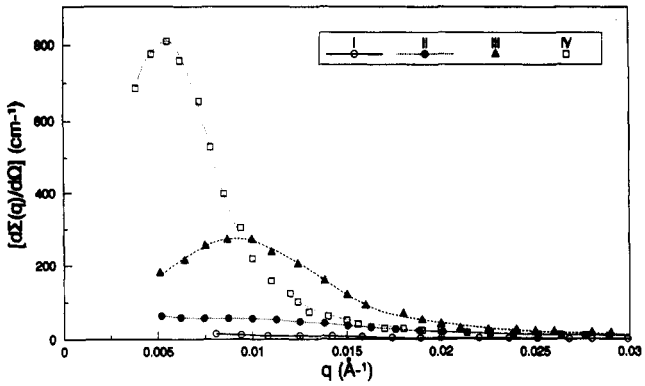

Figure 10. Stages of spinodal decomposition for SCPE64h/dPMMA185 blend 9: (I) single-phase blend is present; (II) phase separation begins (same data set as (●) in Figure 9 above); (III) concentration difference between the phases increases but the phase size remains constant; (IV) phase separation continues and phase size increases. The lines through the experimental points are guides to the eye.

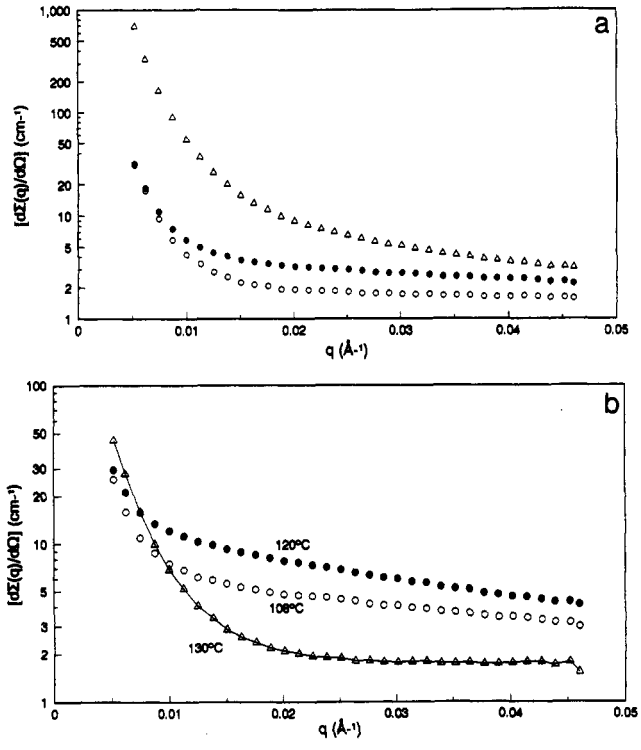

Figure 11. Semilogarithmic plot of $[d\Sigma(q)/d\Omega]^{-1}$ against q for (a) SCPE64h/dPMMA185, blend 11, at three temperatures [(○) 95 °C, (●) 120 °C, and (△) 150 °C] and (b) SCPE66/dPMMA810, blend 3, at three different temperatures [(○) 108 °C, (●) 120 °C, and (△) 130 °C. The line through the points at 130 °C (△) has been drawn for clarity.

the blend in Figure 11b (blend 3 at 130 °C) only shows scattering at low q values, suggesting much more homogeneous phases in the system, with short wavelength concentration fluctuations of very small amplitude.

Thus we have shown what spinodal decomposition looks like and that blends phase separate by nucleation and growth when the blend composition is far from the critical composition and the metastable gap is wide. A detailed analysis of some of the data was made with a view to understanding and quantifying the excess scatter at low q observed from samples which were at temperatures within the miscible region of the phase diagram, as for example in Figure 12. In this example, while for a 25% SCPE composition data of $[d\Sigma(q)/d\Omega]^{-1}$ *vs* q^2 are linear, for a 50% SCPE sample data at low q deviate from linearity. It was found convenient to split the scattering

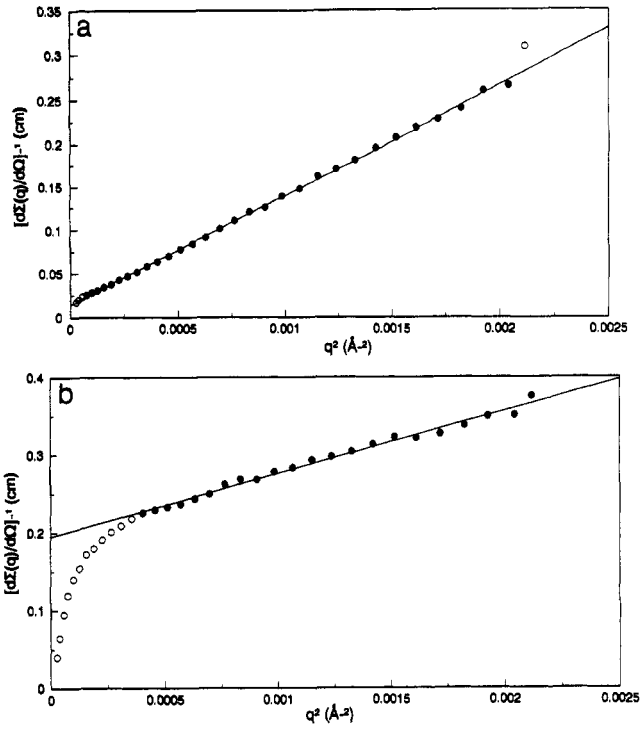

Figure 12. Plots of $[d\Sigma(q)/d\Omega]^{-1}$ against q^2 for SCPE66/dPMMA810 blends: (a) blend 2 at 103 °C; (b) blend 3 at 108 °C. The full circles correspond to the points that were used for the least squares fit.

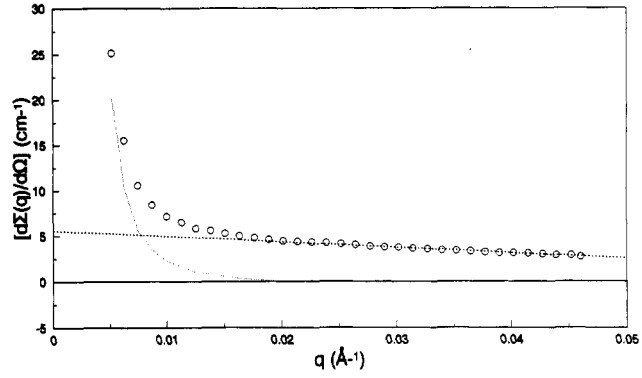

Figure 13. SANS for SCPE66/dPMMA810, blend 3, at 108 °C: (○) $[d\Sigma(q)/d\Omega]_{expt}$; (- - -) $[d\Sigma_1(q)/d\Omega]$; (···) $[d\Sigma_2(q)/d\Omega]$.

curve into two components (Figure 13); each component could be modeled by a well-known scattering law:[50]

$$\left[\frac{d\Sigma(q)}{d\Omega}\right]_{expt} = \frac{d\Sigma_1(q)}{d\Omega} + \frac{d\Sigma_2(q)}{d\Omega} \qquad (17)$$

The first term in eq 17 corresponds to the equilibrium concentration fluctuations in the one-phase blend (*i.e.* eq 3), and the second term models the large scattering obtained at low q values for phase separated systems (*i.e.* eq 13). The term $[d\Sigma_1(q)d\Omega]$ was obtained by fitting the data at high q values where $[d\Sigma_1(q)/d\Omega]^{-1} \propto q^2$ and $[d\Sigma_2(q)/d\Omega]^{-1} \approx 0$. Subsequently, $[d\Sigma_2(q)/d\Omega]$ was found by difference $[(d\Sigma(q)/d\Omega)_{expt} - d\Sigma_1(q)/d\Omega)]$. While $[d\Sigma_1(q)/d\Omega]$ is consistently dependent on temperature, $[d\Sigma_2(q)/d\Omega]$ is apparently independent of temperature until an annealing temperature of above 120 °C (see Figure 14). This type of behavior was noted for blends 3, 10, and 11. With the exceptions of blends 10 at 130 °C and 11 at 150 °C, the $[d\Sigma_2(q)/d\Omega]$ scattering components for the blends with excess low q scattering could be fitted using the Debye–Bueche scattering law described in eq 13 (see Figure 15). Values for the correlation length a were obtained, and they ranged from 130 to 950 Å depending on the blend

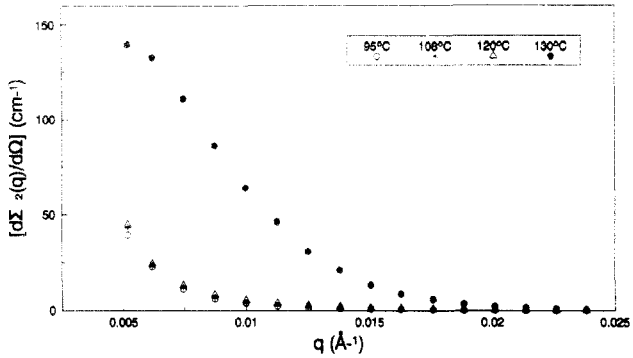

Figure 14. Plot of $[d\Sigma_2(q)/d\Omega]$ against q for the system SCPE64/dPMMA185, blend 10.

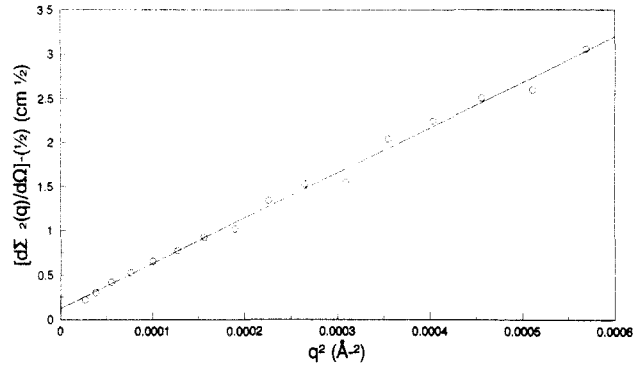

Figure 15. Plot of $[d\Sigma_2(q)/d\Omega]^{-0.5}$ against q^2 for the system SCPE66/dPMMA810, blend 3, at 97 °C. The solid line corresponds to the best fit through the data points.

and on the temperature, and it was observed that the value of a decreased systematically with increasing temperature. There are large errors associated with these values because of the relatively few data points in the fitting range and the number of steps, each with an associated error, in calculating $[d\Sigma_2(q)/d\Omega]$. Because of this, a detailed discussion on the relationship between correlation length and the annealing temperature will not be attempted. However, there may be some significance in the observation that the a values for the two blends of 50% SCPE studied are roughly the same and that they are larger than those for the 75% SCPE blend.

Debye–Bueche scattering behavior is indicative of a random, two-phase structure. We must ask how this two-phase structure can arise in blends at temperatures where other experiments suggest a one-phase material. The $[d\Sigma_2(q)/d\Omega]$ scattering below the phase boundary must be due to some type of large, temperature independent concentration fluctuations. Similar Debye-Bueche scattering behavior has been observed in solutions of polystyrene and perdeuterio polystyrene in benzene, and this scattering behavior, which was unexpected in a solution, was associated with the presence of large scale concentration fluctuations. These large fluctuations were dependent on the sample preparation as well as on concentration.[51]

It is possible that the heterogeneities in the SCPE-rich blends arise during the solution casting of the blends due, for example, to a miscibility gap in the polymer–polymer–solvent phase diagram. If there was an unstable or metastable region in the phase diagram through which only compositions rich in SCPE would pass as the solvent evaporates off, a two-phase structure might be set up in blends of selected concentrations; blends rich in dPMMA might avoid the metastable zone and thus remain homogeneous. This heterogeneous structure would be impossible to anneal out until the sample was heated above T_g. There is no direct observation of this kind of phase behavior in SCPE/dPMMA/solvent mixtures, although this type of ternary phase diagram has been observed in other blend systems, *e.g.* polystyrene/poly(vinyl methyl ether)[52] and PVC/SCPE (43% chlorination).[53]

The sudden increase in the intensity of the $[d\Sigma_2(q)/d\Omega]$'s for annealing temperatures above 130 °C (for blends 3 and 10 and above 150 °C for blend 11) and the finding that two of these blends could not be modeled with the Debye–Bueche function suggest that at these temperatures the blends have begun to phase separate. Since these temperatures are below the spinodal phase boundaries and the scattering curves are not typical of a spinodal phase separation, it is more probable that the phase separation is taking place by nucleation and growth rather than by spinodal decomposition. The inhomogeneities already present in the blends are likely nucleation sites. It is worth pointing out that the interaction parameters obtained for the samples which contain inhomogeneities in the one-phase region of the phase diagram (*i.e.* SCPE-rich blends) correspond to the values for χ for an average composition between those of the microphases present in the system. The values obtained for χ for the dPMMA-rich samples correspond to the nominal blend composition.

Conclusions

The miscibility of blends of deuterated poly(methyl methacrylate) with solution chlorinated polyethylene has been studied by small angle neutron scattering. Interaction parameters and spinodal curves have been obtained as a function of chlorination level of SCPE, composition, and molecular weight of both dPMMA and SCPE.

The chlorination level of the SCPEs has been found to influence miscibility much more than the molecular weight of either dPMMA or SCPE. This points to the large effect that the specific interactions have in this system. The polymer–polymer interaction parameter has been found to be temperature, composition, and molecular weight dependent.

For certain compositions evidence has been found for incompatibility in the three-component polymer–polymer–solvent system during sample preparation. The scattering behavior of such samples has been interpreted in the light of two-phase scattering models.

References and Notes

(1) Shibayama, M.; Yang, H.; Stein, R. S.; Han, C. C. *Macromolecules* **1985**, *18*, 2179.
(2) Higgins, J. S.; Fruitwala, H. A.; Tomlins, P. E. *Br. Polym. J.* **1989**, *21*, 247.
(3) Varnell, D. F.; Moskala, E. J.; Painter, P. C.; Coleman, M. M. *Polym. Eng. Sci.* **1983**, *23*, 658.
(4) Schurer, J. W.; de Boer, A.; Challa, G. *Polymer* **1975**, *16*, 201.
(5) Fowkes, F. M.; Tischler, D. O.; Wolfe, J. A.; Lannigan, L. A.; Ademu-John, C. M.; Halliwell, M. J. *J. Polym. Sci., Polym. Chem. Ed.* **1984**, *22*, 547.
(6) Vorenkamp, E. J.; Challa, G. *Polymer* **1988**, *29*, 86.
(7) Parmer, J. F.; Dickinson, L. C.; Chien, J. C. W.; Porter, R. S. *Macromolecules* **1989**, *22*, 1078.
(8) Garton, A.; Aubin, M.; Prud'homme, R. E. *J. Polym. Sci., Polym. Lett. Ed.* **1983**, *21*, 45.
(9) Allard, D.; Prud'homme, R. E. *J. Appl. Polym. Sci.* **1982**, *27*, 559.
(10) Lemieux, E.; Prud'homme, R. E.; Forte, R.; Jérôme, R.; Teyssié, P. *Macromolecules* **1988**, *21*, 2148.
(11) Hill, R. G.; Tomlins, P. E.; Higgins, J. S. *Marcomolecules* **1985**, *18*, 2555.
(12) Chai, Z.; Lianghe, S.; Sheppard, R. N. *Polymer* **1984**, *25*, 364.
(13) Walsh, D. J.; Higgins, J. S.; Chai, Z. *Polym. Commun.* **1982**, *23*, 336.
(14) Higgins, J. S.; Stein, R. S. *J. Appl. Crystallogr.* **1978**, *11*, 346.
(15) Warner, M.; Higgins, J. S.; Carter, A. J. *Macromolecules* **1983**, *16*, 1931.

(16) Higgins, J. S. In *Polymer Blends and Mixtures*; Walsh, D. J., Higgins, J. S., Maconnachie, A., Eds.; NATO ASI Series; Martinus Nijhoff Publishers: Dordrecht, The Netherlands, 1984; Chapter 5, p 69.
(17) Maconnachie, A.; Fried, J. R.; Tomlins, P. E. *Macromolecules* **1989**, *22*, 4606.
(18) Guinier, A.; Fornet, G. In *Small Angle Scattering of X-rays*; Wiley, New York, 1955.
(19) Zimm, B. H. *J. Chem. Phys.* **1948**, *16*, 1093.
(20) deGennes, P. G. *Scaling Concepts in Polymer Physics*; Cornell University Press: Ithaca, New York, 1979.
(21) Binder, K. *J. Chem. Phys.* **1983**, *79*, 6387.
(22) Cahn, J. W.; Hilliard, J. E. *J. Chem. Phys.* **1958**, *28*, 258.
(23) de Gennes, P.-G. *J. Chem. Phys.* **1980**, *72*, 4756.
(24) Pincus, P. *J. Chem. Phys.* **1981**, *75*, 1986.
(25) Higgins, J. S.; Dawkins, J. V.; Taylor, G. *Polymer* **1980**, *21*, 627.
(26) Debye, P.; Bueche, A. M. *J. Appl. Phys.* **1949**, *20*, 518.
(27) Debye, P.; Anderson, H. R.; Brumberger, H. *J. Appl. Phys.* **1957**, *28*, 679.
(28) Kratky, O. *Pure Appl. Chem.* **1966**, *12*, 483.
(29) Hill, R. G. Ph.D. Thesis, Imperial College, 1985.
(30) Guo, W. Ph.D. Thesis, Imperial College, 1989.
(31) Chai, Z. Ph.D. Thesis, Imperial College, 1982.
(32) Prentice, P. *J. Mater. Sci.* **1985**, *20*, 1445.
(33) ISIS User Guide Experimental Facilities at ISIS. RAL-88-030; Rutherford Appleton Laboratory: Oxfordshire, U.K., Feb 1988.
(34) *LOQ Users' Manual*; Rutherford Appleton Laboratory: Oxfordshire, U.K., 1988.
(35) Ghosh, R. E. A Computer Guide for Small Angle Scattering Experiments; Technical Report No. 89GH02T; Institut Max Von Laue Paul Langevin; Grenoble, France, 1989.
(36) Gabrys, B.; Tomlins, P. E. *Encyclopedia of Polymer Science and Engineering*, 2nd ed.; John Wiley & Sons: New York, 1989; Vol. 15.
(37) Kirste, R. G.; Oberthur, R. C. In *Small Angle in X-ray Scattering*; Glatter, O., Kratky, O., Eds.; Academic Press: New York, 1982; Chapter 12, p 405.
(38) Ullman, R. *J. Polym. Sci., Polym. Phys. Ed.* **1985**, *23*, 1477; *J. Polym. Sci., Polym. Lett. Ed.* **1983**, *21*, 521.
(39) Boue, F.; Nierlick, M.; Leibler, L. *Polymer* **1982**, *23*, 29.
(40) Crist, B.; Graessley, W. W.; Wignal, G. D. *Polymer* **1982**, *23*, 1561.
(41) Dettenmaier, M.; Maconnachie, A.; Higgins, J. S.; Kausch, H. H.; Nguyen, T. Q. *Macromolecules* **1986**, *19*, 773.
(42) Fox, T. G. *Bull. Am. Phys. Soc.* **1956**, *1*, 123.
(43) Han, C. C.; Bauer, B. J.; Clark, J. C.; Muroga, Y.; Matsushita, Y.; Okada, M.; Tran-cong, Q.; Chenag, T.; Sanchez, I. C. *Polymer* **1988**, *29*, 2002.
(44) Higgins, J. S.; Fruitwala, H.; Tomlins, P. E. *Macromolecules* **1989**, *22*, 3674.
(45) Brereton, M. G.; Fischer, E. W.; Herkt-Maetzky, Ch.; Mortensen, K. *J. Chem. Phys.* **1987**, *87*, 2144.
(46) Bates, F. S.; Dierker, S. B.; Wignall, G. D. *Macromolecules* **1986**, *19*, 1938.
(47) Koch, T.; Strobl, G. R. *J. Polym. Sci., Polym. Phys. Ed.* **1990**, *28*, 343.
(48) Fruitwala, H. Ph.D. Thesis, Imperial College, 1988.
(49) Murray, C. T.; Gilmer, J. W.; Stein, R. S. *Macromolecules* **1985**, *18*, 996.
(50) Hahn, K.; Schmitt, B. J.; Kirschey, M.; Kirste, R. G.; Salie, H.; Schmitt-Strecker, S. *Polymer* **1992**, *33*, 5150.
(51) Koberstein, J. T.; Picot, C.; Benoit, H. *Polymer* **1985**, *26*, 673.
(52) Robard, A.; Patterson, D.; Delmas, G. *Macromolecules* **1977**, *10*, 706.
(53) Rueda de la Garza, G. Ph.D. Thesis, Imperial College, 1987.
(54) Khambatta, F. B.; Warner, F.; Russell, T.; Stein, R. S. *J. Polym. Sci., Polym. Phys. Ed.* **1976**, *14*, 1391.